AGU PUBLICATIONS

JGR

Journal of Geophysical Research: Oceans

RESEARCH ARTICLE

10.1002/2014JC010330

Key Points:

- Chl-a phenological indexes displayed submesoscale and mesoscale variability
- Few interannual changes in Chl-a phenology were detected
- Mean Chl-a annual cycle was coupled to those of ZET and PAR

Correspondence to:
C. E. Morales,
camorale@udec.cl

Citation:
Corredor-Acosta, A., C. E. Morales, S. Hormazabal, I. Andrade, and M. A. Correa-Ramirez (2015), Phytoplankton phenology in the coastal upwelling region off central-southern Chile (35°S–38°S): Time-space variability, coupling to environmental factors, and sources of uncertainty in the estimates, *J. Geophys. Res. Oceans*, *120*, 813–831, doi:10.1002/2014JC010330.

Received 22 JUL 2014
Accepted 7 JAN 2015
Accepted article online 19 JAN 2015
Published online 12 FEB 2015

Phytoplankton phenology in the coastal upwelling region off central-southern Chile (35°S–38°S): Time-space variability, coupling to environmental factors, and sources of uncertainty in the estimates

Andrea Corredor-Acosta[1], Carmen E. Morales[2], Samuel Hormazabal[3], Isabel Andrade[3], and Marco A. Correa-Ramirez[3]

[1]Postgraduate Program in Oceanography and Instituto Milenio de Oceanografía, Universidad de Concepción, Concepción, Chile, [2]Instituto Milenio de Oceanografía, Department of Oceanography, Universidad de Concepción, Concepción, Chile, [3]Escuela de Ciencias del Mar and Instituto Milenio de Oceanografía, Pontificia Universidad Católica de Valparaíso, Valparaíso, Chile

Abstract The annual cycle and phenology of phytoplankton (satellite-derived chlorophyll-a, Chl-a) in the coastal upwelling region off central-southern Chile, their time-space variation, the extent of their coupling with those of wind-driven upwelling (as Zonal Ekman Transport, ZET), Sea Surface Temperature (SST), and Photosynthetically Active Radiation (PAR) were analyzed using a ~10 year satellite time series (2002–2012). Wavelet analysis (WA) was applied to extract the dominant frequencies of variability and their recurrence, to derive the phenological indexes, and to assess the extent of the coupling between Chl-a and environmental forcing in the annual frequency. Index estimates were obtained from minimum and maximum accumulated values in two different frequency bands, annual (WA-ANF) and all except the synoptic (WA-ALF). The annual frequency was dominant in all the variables; however, the annual cycle and phenology of Chl-a displayed higher submeso and mesoscale variability. The mean onset date of Chl-a was similar to those of PAR and ZET with WA-ALF and cross WA indicated that, for the most part, their annual cycles were coupled or coherent. Few interannual changes in Chl-a phenology were detected, including a ~1 month longer duration (WA-ALF) during La Niña 2010–2011. The mean anomalies in the magnitudes of Chl-a and ZET during the upwelling season showed a slight but significant trend, negative for Chl-a and positive for ZET, while SST remained relatively constant. This pattern was unexpected since three La Niña-related conditions were identified during the 2007–2012 period.

1. Introduction

Phytoplankton phenology, focused on the potential shifts in the timing, spatial extension, and phase of annual blooms, has been a subject of intensive research in the last decade because of its relevance in the characterization of the biological responses to environmental change and climate fluctuations [*Edwards and Richardson*, 2004; *Thackeray et al*., 2012] and in the assessment of the state of aquatic ecosystems [*Cole et al*., 2012; *Racault et al*., 2014]. As an example of its importance, a delay in the annual start of phytoplankton bloom could produce a mismatch in terms of food availability to higher trophic levels [e.g., *Edwards and Richardson*, 2004; *Gomez et al*., 2012]. Ways to better quantify and monitor shifts in plankton phenology have been suggested, including improvements of the statistical tools for identifying the timing of the periodic behavior and in the separation of time from space changes in this timing [*Ji et al*., 2010].

Studies of phytoplankton phenology have been carried out using in situ or satellite time series of abundance or biomass data. In situ time series provide the means for detailed characterizations of community and species-specific interannual or longer-term changes in the annual cycle of phytoplankton in freshwater and marine coastal ecosystems [e.g., *Winder and Cloern*, 2010; *Kim et al*., 2009]. While satellite time series do not provide detailed characterizations, they do offer wide temporal and spatial coverage [*Platt and Sathyendranath*, 2008; *Platt et al*., 2009; *Land et al*., 2014]. Most of the phenological studies based on in situ time series have focused on coastal waters [*Kim et al*., 2009; *Winder and Cloern*, 2010] because of sampling constraints whereas most of the satellite-based studies have been of open ocean waters [e.g., *Sapiano et al*., 2012; *Racault et al*., 2012] and, in a few cases, coastal systems [e.g., *Henson and Thomas*, 2007a, 2007b; *Zhai et al*., 2011], probably because the signal in the latter can be noisy due to the presence of other fluorescent material and/or turbidity [*Winder and Cloern*, 2010].

The phenology of phytoplankton has usually been described in terms of indexes, such as the onset or initiation, end or termination, duration, and amplitude of the bloom during the annual cycle [*Platt and Sathyendranath*, 2008; *Ji et al*., 2010]. Various methods have been used to derive these indexes from time series with or without data gaps [e.g., *Cole et al*., 2012; *Brody et al*., 2013]. In the estimation of the onset of an annual bloom, differences exceeding 2 months have been found among the most common methods applied with satellite ocean color data (e.g., threshold, rate of change, and cumulative sum methods) [*Brody et al*., 2013]. For its part, wavelet analysis (WA) has not been applied for these purposes with phytoplankton time series, but only to describe the dominant frequencies of variability in them [*Winder and Cloern*, 2010]. WA has been proposed for phenological studies because it deals adequately with time series in which there are changes in the timing of periodic behavior (i.e., nonstationary) and in which the data are relatively noisy [*Hudson*, 2010; *Carl et al*., 2013], as is the case of phytoplankton time series [*Winder and Cloern*, 2010].

For time series that contain gaps in the data, the interpolation technique employed to fill these gaps has also been shown to have an effect on index estimation [e.g., *Cole et al*., 2012; *Brody et al*., 2013; *Land et al*., 2014]. Among them, the Data Interpolating Empirical Orthogonal Function (DINEOF) [*Beckers and Rixen*, 2003; *Alvera-Azcárate et al*., 2005, 2007] has been proposed as an adequate method because it interpolates both in time and space, is parameter free, and allows a rapid reconstruction of missing information without the need for a priori information about the data [*Alvera-Azcárate et al*., 2011]. However, there have been few applications of DINEOF to ocean color time series [*Miles and He*, 2010; *Correa-Ramirez et al*., 2012; *Wang and Liu*, 2014]. Overall, differences in the approaches used in Chl-a phenological studies make time-space comparisons difficult and may also affect the evaluation of the coupling to environmental forcing in a given region [*Ji et al*., 2010; *Winder and Cloern*, 2010; *Brody et al*., 2013].

In the Humboldt Current System (HCS), coastal upwelling is highly seasonal in the region off central-southern Chile ($\sim$33°S–42°S) [*Strub et al*., 1998] and is strongly associated with phytoplankton bloom formation during the austral spring-summer [*Yuras et al*., 2005; *Correa-Ramirez et al*., 2012; *Morales et al*., 2013]. *Montecinos and Gomez* [2010] analyzed the phenology of coastal upwelling (in terms of the cumulative sum method for ZET) for the area off Concepción ($\sim$36.5°S), using in situ (airport at Carriel Sur) and satellite wind (QuikSCAT) time series data. They found interannual variations associated with El Niño-Southern Oscillation (ENSO), with shorter (longer) duration of the annual cycle and weaker (stronger) intensity of upwelling favorable ZET during El Niño (La Niña) events. Based on these results and the well-recognized association between coastal upwelling and phytoplankton blooms in the area off Concepción [e.g., *Escribano and Morales*, 2012], we expected Chl-a phenology to display a similar pattern of ENSO-related interannual change and this in turn produce a major impact on biological productivity in the region. This study focuses on the characterization of phytoplankton (satellite-derived Chl-a) annual cycle and phenology in the coastal upwelling region between 35°S and 38°S, including their time-space variations, and on the extent of their coupling to potential environmental forcing (SST, ZET, and PAR). For this purpose, a $\sim$10 year satellite time series (2002–2012) was analyzed, using DINEOF interpolation to fill gaps in the time series and WA to identify the dominant periods of variability and their recurrence, to derive the phenological indexes, and to assess the coherence between the annual cycles and phenology of Chl-a with those of environmental variables. In addition, a comparison of the WA method to obtain the phenological indexes was done using WA in the annual frequency band and WA for all the frequencies except the synoptic, and other common methods.

2. Data and Methods

2.1. Satellite Time Series

High temporal and spatial resolution of satellite time series data are required to reduce uncertainty in the estimation of phenological indexes [e.g., *Foukal and Thomas*, 2014]. This is especially important for the region off central-southern Chile since: (a) the interannual differences in ZET indexes are of the order of $\sim$15–30 days [*Montecinos and Gomez*, 2010], and (b) the annual cycle of Chl-a in the coastal zone displays a complex pattern, associated with variations in coastline orientation and bathymetry [*Correa-Ramirez et al*.,

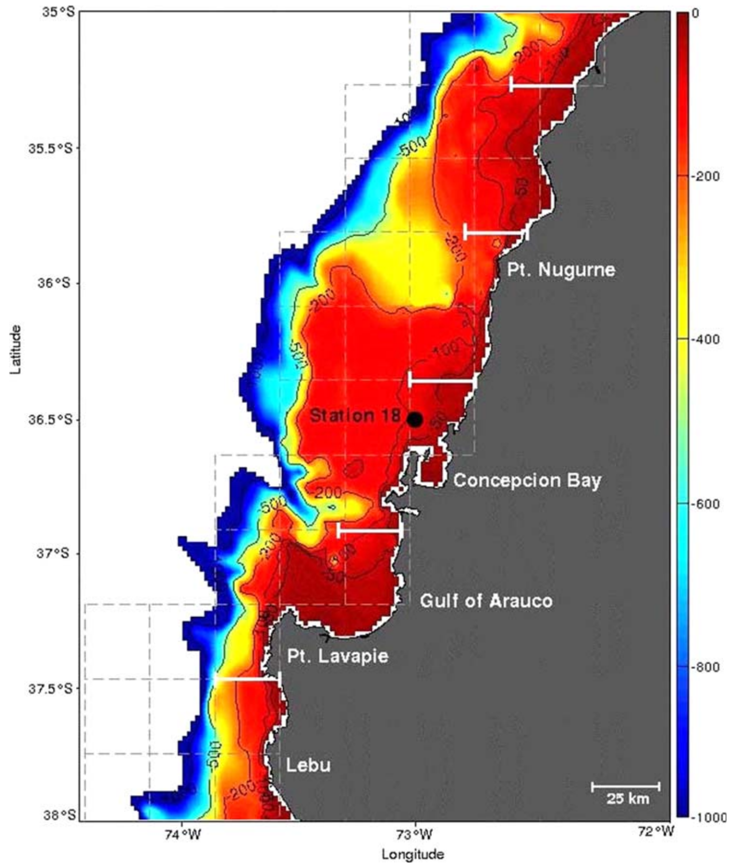

Figure 1. Study area in central-southern Chile (35°S–38°S), including bathymetry and topographic features. The grids (25 × 25 km^2; gray broken lines) denote the three pixels used in the analysis of satellite wind data, the coastal pixel being the one closest to the coast (<30% composed of land surface). The white bars perpendicular to the coast exemplify the first 25 km from the coast for Chl-a and SST data (1 × 1 km resolution). The black dot marks the location of the COPAS coastal time series Station 18 (36°30.80′S, 73°7.75′W; ~90 m depth).

2012; *Morales et al*., 2013]. Satellite time series data of surface Chl-a, ZET, SST, and PAR were analyzed for the coastal region between 35°S and 38°S, and from the coast to ~75 km offshore (Figure 1). Daily values of Chl-a (OC4 algorithm) and SST, with a spatial resolution of ~1 × 1 km, were obtained from level-2 products of the Moderate Resolution Imaging Spectro-radiometer—MODIS-Aqua mission (http://oceancolor.gsfc.nasa.gov/) during the period between 19 July 2002 and 17 May 2012. In terms of data validation, a reasonable agreement between in situ Chl-a (fluorometry and HPLC) and satellite Chl-a data has been reported for the region of study [*Stuart et al*., 2004].

Daily PAR data (9 × 9 km resolution) were also obtained from level-3 products of the MODIS-Aqua mission (http://oceancolor.gsfc.nasa.gov/) from 4 July 2002 to 31 December 2012. Daily surface wind data, with a spatial resolution of 25 × 25 km, were acquired from the product CCMP L3.0 (Cross-Calibrated, Multi-Platform Ocean Surface Wind Velocity) from 1 July 2002 to 31 December 2011. This product integrates measurements from the following missions: SSM/I, SSMIS, AMSR-E, TRMM TMI, QuikSCAT, SeaWinds, and WindSat (http://podaac.jpl.nasa.gov/). For ZET calculation [*Bakun and Nelson*, 1991], satellite wind data corresponding to the 18:00 h (GMT) set (14:00 local time) were selected as representative of daily values in terms of upwelling/downwelling conditions. Wind data from the three pixels nearest the coast (covering the first ~75 km from the coast) were used to calculate ZET, but the pixel nearest the coast (<30% composed of land surface) was equally representative of wind forcing, as was found in the preliminary analyses. ZET data were rotated with respect to the angle of the topography of the continental margin and the series were multiplied by −1 so that positive (negative) values imply offshore (onshore) ZET or upwelling (downwelling) conditions.

2.2. Filling Data Gaps in the Time Series

The gaps in the region of study during the 2002–2012 Chl-a satellite time series are relatively large (~50–60%), but do not show a seasonal pattern; the mean duration of the gaps between valid data is ~2.5–3 days [*Morales et al*., 2013]. For SST, we assume it is the same because the data come from the same source, whereas gaps in the wind and PAR time series are minimal (<7 and <1%, respectively). The mean duration of gaps in the Chl-a and SST time series implies that there at least two valid data per week in each pixel; this would enable the detection of oscillations with a maximum frequency of 6 days (Nyquist frequency). Since the phase of the oscillation is unknown, a doubling in the number of valid data is required; this translates into an uncertainty of ~2 weeks in the detection of the phenological indexes in the Chl-a and SST time series.

Gaps in the Chl-a and SST time series were filled through interpolation using DINEOF in its univariate mode [*Alvera-Azcárate et al*., 2005, 2007], following the approach in *Correa-Ramirez et al*. [2012] of using a window of 31 days for the iterations of data from the Peru-Chile system. Essentially, DINEOF consists of a series of iterations to calculate the field values at missing positions. First, spatial and temporal means are removed from the data and the missing data are initialized to zero. The first EOF is calculated from this field and the missing data are replaced with the values obtained by EOF decomposition. This procedure is repeated until a convergence criterion for the missing data values is reached; in our case, this criterion was achieved when the percentage of the error estimated from cross validation was less than 10%. After that, the second EOF is calculated and the whole procedure is repeated, and so on. The total number of EOFs to be calculated is determined by cross validation and depends on the amount of valid data in the window selected for the iterations (details in *Alvera-Azcárate et al*. [2011]). This total fluctuated between three and eight EOFs in our case.

2.3. Annual Cycles, Phenological Indexes, and Coupling Assessment

The mean annual cycles of Chl-a, SST, ZET, and PAR in the region of study were characterized through harmonic analysis in the annual frequency and through the monthly mean climatology of these variables. The latitudinal and zonal variability of the monthly mean climatology of Chl-a was also graphically analyzed. In addition, WA was applied to extract the dominant frequency bands (as a band-pass filter) and their recurrence in the time series, as well as to derive the phenological indexes of the variables, and to assess the coupling of Chl-a to environmental forcing. WA performs a time-frequency decomposition of the signal by estimating its spectral characteristics as a function of time [*Torrence and Compo*, 1998; *Grinsted et al*., 2004]. For this purpose, the continuous Morlet wavelet transform was applied to normalized time series data to obtain the wavelet power spectrum of the different variables, using the MATLAB functions provided by *Torrence and Compo* [1998] (http://atoc.Colorado.edu/research/wavelets/) and *Grinsted et al*. [2004]. The significance of the frequency bands was evaluated with Monte Carlo experiments (95% confidence, 1000 iterations). Details of the WA applied to study phytoplankton blooms have been summarized in *Winder and Cloern* [2010].

The definitions of the phenological indexes used in this study followed those described in previous studies based on satellite Chl-a [e.g., *Platt and Sathyendranath*, 2008; *Racault et al*., 2012] and on ZET accumulated data [*Bograd et al*., 2009; *Montecinos and Gomez*, 2010]:

1. Onset or initiation, Julian date when the annual cycle of a variable achieves a minimum accumulated value, which marks the beginning of this cycle; for ZET, this index refers to the beginning of the offshore ZET or upwelling season (see section 2.1).
2. End or termination, Julian date when the annual cycle of a variable achieves a maximum accumulated value.
3. Duration, equivalent to the number of days between the onset and the end dates.
4. Amplitude, the accumulated magnitude value between the onset and end.

The estimation of the phenological metrics from minimum (onset) and maximum (end) accumulated values was based on the reconstruction, from wavelet transform, of the annual frequency band (WA-ANF), and of all the frequency bands except the synoptic (WA-ALF), the latter often being used in other commonly applied index estimation methods [*Brody et al*., 2013]. In preliminary analyses, the results of using all frequencies (1–1024 days) were similar to those obtained using all the frequencies except the synoptic (16–1024 days); however, the latter was chosen considering the level of uncertainty in the Chl-a data (see section 2.2). In addition, index estimation with WA was compared with other commonly used methods. First, the threshold method for the estimation of Chl-a onset was applied, following *Henson and Thomas* [2007a] and using DINEOF-interpolated data; an 8 day filter was used to smooth out the high-frequency data and a threshold value was calculated (5% increase in Chl-a concentration with respect to the annual median value in each year and for the whole time series). In this method, the onset corresponds to the first date at which the threshold value is attained and maintained for at least 3 days. Second, the cumulative sum method for ZET onset and end was applied; the indexes were obtained from the minimum (onset) and maximum (end) values in raw time series of accumulated data [*Bograd et al*., 2009; *Montecinos and Gomez*, 2010]. In each case, the phenological year was considered from 1 July of year-N until 30 June of the year-N + 1.

In assessing the extent of coupling or coherence between the annual cycle of Chl-a with each of the environmental variables (SST, ZET, and PAR), cross wavelet and phase analysis (cross WA) was applied. This method allows proper detection of similarities (coherence) and phase differences for each frequency between two time series [*Grinsted et al*., 2004; *Cazelles et al*., 2008; *Hudson*, 2010]. In cross-WA coherence diagrams, the level of covariability between pairs of two time series is represented by values between 0 and 1; the relative phase between the time series is denoted by arrows (right: in phase; left: antiphase; up or down: ones series leads the other by 90° [e.g., *García-Reyes et al*., 2013].

2.4. Time-Space Variability in Phenology

Spatial variability in the phenological indexes of Chl-a, SST, ZET, and PAR was assessed for the latitudinal range between 35°S and 38°S. For this purpose, a mean index value (onset, end, and duration) for each variable at each latitude (1 km apart for Chl-a and SST; 25 km for ZET, and 9 km for PAR) was calculated using the WA-ANF and WA-ALF approaches. In the case of Chl-a, the indexes were also calculated for three different zonal bands: 0–25, 25–50, and 50–75 km from the coast and at each latitude.

Interannual variability in the phenological indexes of Chl-a, SST, ZET, and PAR was explored by calculating regional values (onset, end, duration, and amplitude) for each year in the time series. In addition, annual anomalies in these indexes and their latitudinal distribution were analyzed. To obtain these anomalies, the mean index for each latitude and all years was calculated and subtracted from the index estimated for each year (annual index), which was then normalized (division by the standard deviation combining all years). Furthermore, anomalies in the concentration of Chl-a and in the values of the environmental variables (SST, ZET, and PAR), collectively defined here as magnitude anomalies, were also obtained as above and for each latitude, except that daily values during the productive period of each year (from 1 September year N to 31 March year N + 1) were used. Two types of calculations to obtain mean anomaly values per year were made for the latter case: (i) an annual mean value for the productive period of each year (explained above for the phenological indexes), and (ii) a mean value per month during the productive period of each year (seven values per year).

In order to further explore the factors influencing time-space variability in the phenology of Chl-a, SST, ZET, and PAR, we investigated the role of climatic variability, especially that associated with ENSO (represented by the Multivariate ENSO Index), the Antarctic Oscillation (AAO), and the Pacific Decadal Oscillation (PDO). Data for the MEI, AAO, and PDO were obtained from http://www.esrl.noaa.gov/psd/data/correlation/mei.data, http://www.cpc.ncep.noaa.gov/products/precip/CWlink/daily_ao_index/aao/monthly.aao.index.b79.current.ascii.table, and http://jisao.washington.edu/pdo/PDO.latest, respectively. Moving averages (3 months) during the productive period, centered on the corresponding month of Chl-a anomalies, were calculated with these data. Anomalies in the magnitude of each variable were obtained as above but on a monthly basis within the productive period (seven data points per year, each representing 1 month). In each case, a trend was calculated by fitting a linear regression. In addition, anomalies of in situ time series data were used to complement the satellite information. Daily in situ wind data from the Carriel Sur airport (provided by the Meteorological Direction of Chile via A. Montecinos) was used to calculate ZET anomalies, as above. Monthly in situ data from a fixed time series station on the shelf off Concepcion (Station 18, 36°30.80′S, 73°7.75′W) was also used to derive the SST and density (sigma-t) anomalies. The latter data were used to calculate a stratification index (0–50 m depth), following *Simpson et al*. [1982].

3. Results

3.1. Annual Cycle of Chl-a and of Environmental Variables in the Region of Study

The raw data from the Chl-a time series (2002–2012) in the coastal upwelling region (between 35°S and 38°S, and from the coast to 75 km offshore) displayed strong annual fluctuations (higher mean values in the austral spring-summer and lower values in autumn-winter). The same patterns were observed in the raw data from the SST, ZET, and PAR time series (Figures 2a–2d). The mean annual cycle of each of the variables (annual harmonic and monthly mean climatology) are represented in Figures 2e–2h. The mean annual cycle of Chl-a attained maximum values ($\geq$3.5 mg m^{-3}) during the austral spring-summer (October–

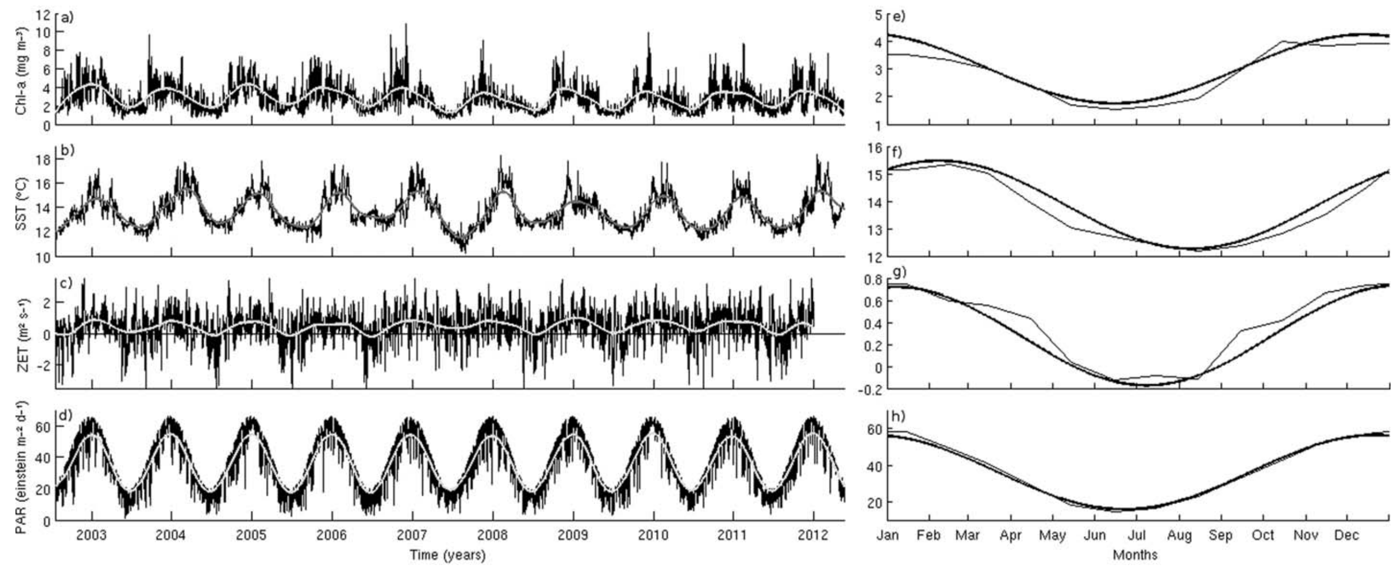

Figure 2. (a–d) Daily satellite time series (mid-2002 to mid-2012) data and (e–h) annual cycles of the variables in the region of study, the latter represented by monthly mean climatologies (thinner lines) and annual harmonic curves (thicker lines). The gray lines in the Chl-a, SST, ZET, and PAR time series data (Figures 2a–2d) represent 3 month moving averages; the *y* axis names and units apply for both left and right figures in each variable and the *x* axis tics mark the beginning of each month.

January) and minimum values ($\leq$2 mg m^{-3}) during the autumn-winter (May–July). The cycles of ZET and PAR achieved their maxima from November to February ($\geq$0.6 m^2 s^{-1} and $\geq$50 Einstein m^{-2} d^{-1}, respectively) and their minima in winter (close to or below 0 m^2 s^{-1} and $\leq$20 Einstein m^{-2} d^{-1}, respectively). Maximum ($\geq$15°C) and minimum SST values ($\leq$12°C) were attained during December–March and June–September, respectively.

The annual climatological cycle of Chl-a presented both alongshore and across-shore variability in the region of study (Figure 3). The mean annual Chl-a cycle described above was similar at some latitudes (between 36°S and 37°S), but in most cases was shorter in duration north of ~36°S. An upwelling focus (Point Nugurne) is located at this latitude, as well as a marked narrowing in shelf width. A strong discontinuity in the annual cycle is located at ~37.2°S (area of the Gulf of Arauco and immediately south of it, a main

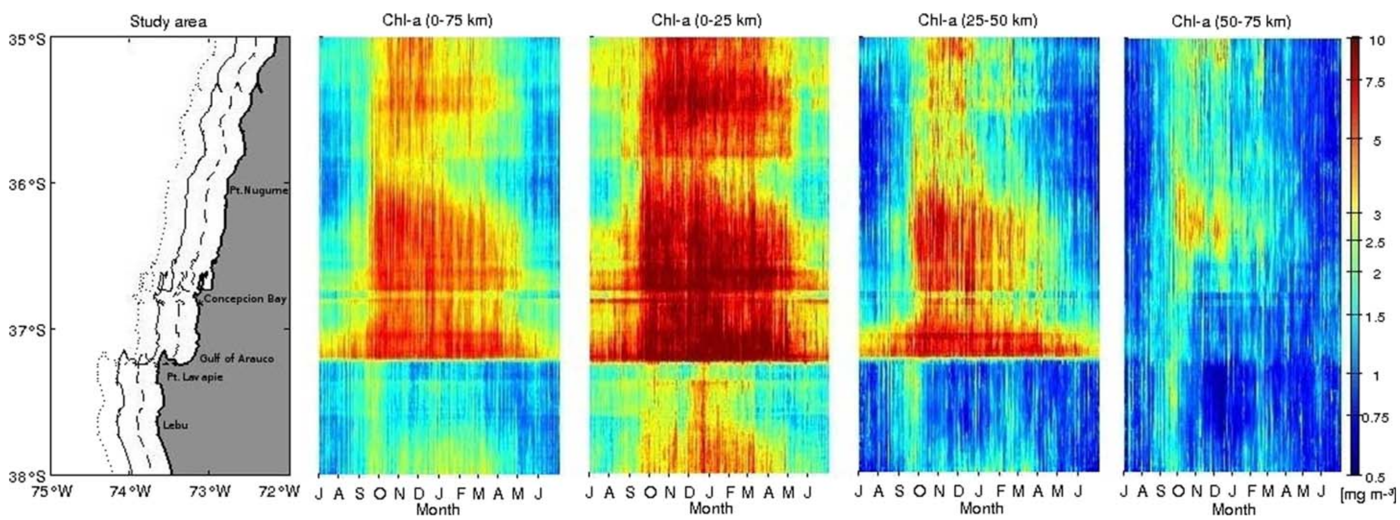

Figure 3. Hovmöller diagram of the latitudinal distribution of the monthly climatology of Chl-a (mid-2002 to mid-2012), including a map of the region (left figure) and, to the right, the mean Chl-a values (mg m^{-3}) in the region (0–75 km) and in the sections 0–25, 25–50, and 50–75 km offshore, respectively. The location of these sections is depicted in the map as successive 25 km projections from the coast.

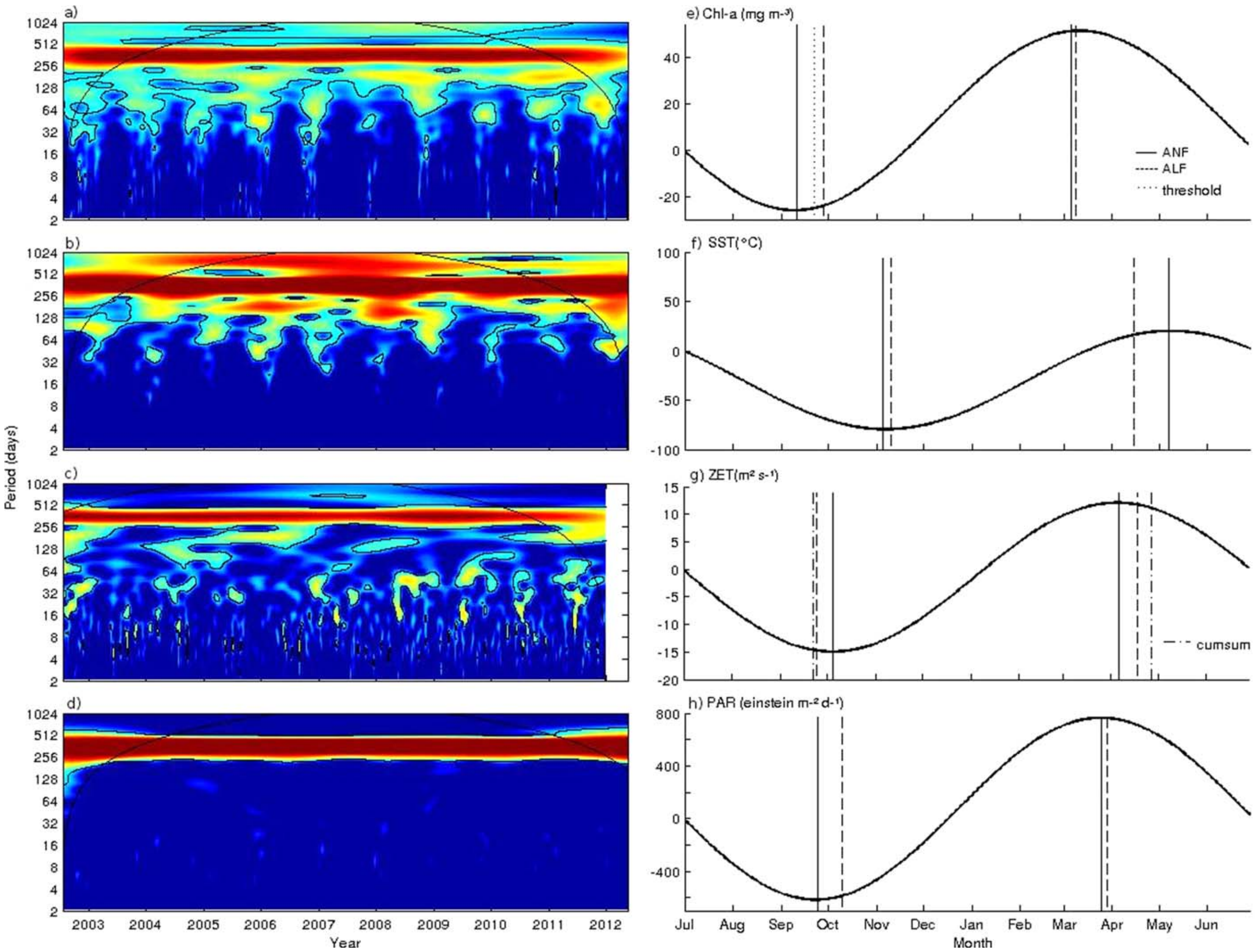

Figure 4. (a–d) Wavelet power spectra of the times series data and (e–h) mean regional phenological indexes derived from WA reconstruction for each of the variables during the period of study (∼2002–2012): Chl-a (Figures 2a and 2e), SST (Figures 2b and 2f), ZET (Figures 2c and 2g), and PAR (Figures 2d and 2h). In the wavelet power spectra, the color scale represents how the strength of the periodicities changes over time (blue indicates weak variance and red indicates strong variance). The thin black contours surrounding regions of stronger variance in the spectra indicate coherent time-frequency regions that are significant (95% significance, Monte Carlo experiments with 1000 iterations); the black curved line in the spectra depicts the cone of influence, outside of which edge effects become important (i.e., data in this area should not be considered). In the phenological curves, ANF and ALF refer to the two frequency bands used in the estimations of the indexes with WA (vertical straight and dotted lines, respectively) for onset (lines to the left) and end (lines to the right); the WA curve represents the reconstructed annual frequency. The indexes derived from the threshold method for Chl-a onset and from cumulative sum method for the onset and end of ZET cycle are also shown.

upwelling focus, Point Lavapie), with lower Chl-a concentrations and weaker seasonality in the area south of it. This discontinuity was also evident when we graphed the offshore band (50–75 km from the coast) off the Gulf of Arauco adjacent to the coastal band (0–25 km from the coast) off Pt. Lavapie (data not shown). The annual Chl-a cycle also showed differences in the across-shore direction, with the highest summer values (∼5 mg m^{-3}) in the coastal band (0–25 km from the coast), with weaker seasonality and the lowest Chl-a values (<1 mg m^{-3}) in the offshore band (50–75 km from the coast), so that the mean annual cycle was highly influenced by the patterns observed in the first 50 km from the coast.

The wavelet power spectrum derived from WA for the time series of all the variables (Figures 4a–4d) revealed that the most dominant and recurrent period of significant variability was in the annual frequency band. The energy in this band spans from 250 to 540 days; this broadband was used in subsequent analyses in order to account for energy leakage between frequencies and the spectral frequency resolution. Intraseasonal variability was second in importance in the case of Chl-a and SST (mostly in the band between ∼60 and 90 days), and less so in the case of ZET (mostly in the band between ∼30 and 60 days); higher-

Table 1. Comparison of the Phenological Indexes for Chl-a Onset and for ZET Onset and End Using Three Different Methods[a]

		Threshold	WA-ALF	Cumulative Sum		WA-ALF	
		Chl-a	Chl-a	ZET		ZET	
Periods	ENSO	Onset	Onset	Onset	End	Onset	End
2002–2003	El Niño	90	87	138	269	107	278
2003–2004	Neutral	85	95	116	270	87	268
2004–2005	Neutral	80	88	68	297	77	297
2005–2006	Neutral	81	78	68	290	83	292
2006–2007	Neutral	52	84	53	314	86	274
2007–2008	La Niña	59	82	119	317	79	316
2008–2009	Neutral	95	103	71	302	86	296
2009–2010	El Niño	92	105	67	340	86	334
2010–2011	La Niña	74	82	58	312	69	313
2011–2012	La Niña	78	92	ND	ND	ND	ND
	Mean	84	90	84 ± 31	301 ± 22	86 ± 12	292 ± 3

[a]The number of Julian days representing the indexes refer to the 1 July (phenological year).

frequency variability (<30 days) occurred irregularly in all the variables. Variability in Chl-a in the ~120 days frequency probably relates to the impact of submeso and mesoscale activity (e.g., eddy generation time, upwelling front formation, etc.) on Chl-a distribution.

3.2. Phenological Indexes for Chl-a and Environmental Variables

Figures 4e–4h show the mean time-space values for the onset and end dates of the annual Chl-a, SST, ZET, and PAR cycles in the region of study, obtained from WA-ANF (250–540 days band), as well as the index estimates derived from other methods (WA-ALF for all the variables, threshold method for Chl-a onset, and cumulative sum for ZET onset and end). In general, the mean indexes derived from the three latter methods were similar whereas those obtained with WA-ANF were markedly different. For example, the onset of the Chl-a bloom was placed in the first half of September with WA-ANF and in the second half of September with WA-ALF and threshold methods; the end, however, was placed at the beginning of March with both WA approaches.

In Table 1, the mean values of the indexes (both time-space means and spatial means per phenological year) obtained with the threshold method (for the onset of Chl-a) and with the cumulative sum (for onset and end ZET) are compared with those obtained with the WA-ALF approach. For the most part, Chl-a onset estimates with both methods were similar, except that an earlier onset (25–30 days) compared to the mean time-space value was observed in 2006–2007 and 2007–2008 with the threshold approach. As for the ZET indexes, differences of up to 30–40 days were found with both methods, although the mean time-space values were very similar. In Table 2, the mean index values (both time-space means and spatial means per phenological year) obtained with the WA-ANF and WA-ALF calculations are shown; differences in index estimation with these frequencies are also evident, as described for Figures 4e–4h.

3.3. Spatial Variability in the Phenological Indexes

The mean regional (0–75 km from the coast) Chl-a indexes calculated with WA displayed submeso and mesoscale (from ~10 to ~100 km) alongshore variability when calculated with WA-ANF (Figure 5a) and WA-ALF (Figure 5c). The distribution of the phenological indexes in the two most coastal zonal sections (0–25 and 25–50 km from the coast) was similar to that observed for the region but different from that in the offshore section (50–75 km from the coast). The most pronounced index differences from the mean pattern were located in the area between ~37.2°S and 37.5°S. This area includes the Gulf of Arauco and the upwelling center at Pt. Lavapie, where coastline orientation and bathymetry are very different from the areas to the north (Figure 1) and where the annual Chl-a cycle displays a strong discontinuity (Figure 3).

Based on these spatial differences in the Chl-a annual cycle and the phenological indexes, the mean indexes for the areas north and south of the 37.2°S discontinuity were estimated using WA-ANF and WA-ALF (Table 3). In general terms, the indexes in both areas were similar (<15 days differences) to the regional mean values with WA-ANF. However, with WA-ALF, a difference was found in Chl-a onset (~29 days), being earlier in the southern area. In the case of the phenological indexes for SST, ZET, and PAR calculated with WA-ANF

Table 2. Interannual Variability and Standard Deviation of the WA-Derived Phenological Indexes for Chl-a, ZET, and PAR in the Region of Study[a]

			Onset			End			Duration			Amplitude	
	Periods	ENSO	Chl-a	ZET	PAR	Chl-a	ZET	PAR	Chl-a	ZET	PAR	Chl-a	ZET
ALF	2002–2003	El Niño	87 ± 25	107 ± 1	99 ± 17	245 ± 17	278 ± 18	270 ± 8	159 ± 32	172 ± 18	171 ± 22	84	12
	2003–2004	Neutral	95 ± 16	87 ± 44	117 ± 3	253 ± 23	268 ± 1	269 ± 1	159 ± 28	182 ± 44	153 ± 3	47	20
	2004–2005	Neutral	88 ± 24	77 ± 5	96 ± 13	244 ± 31	297 ± 1	275 ± 3	157 ± 40	221 ± 6	180 ± 13	60	20
	2005–2006	Neutral	78 ± 41	83 ± 18	109 ± 11	258 ± 31	292 ± 10	272 ± 3	180 ± 42	210 ± 23	164 ± 11	54	21
	2006–2007	Neutral	84 ± 22	86 ± 28	98 ± 16	256 ± 22	274 ± 7	267 ± 2	173 ± 33	188 ± 34	169 ± 16	79	15
	2007–2008	La Niña	82 ± 21	79 ± 46	91 ± 17	246 ± 39	316 ± 1	269 ± 4	165 ± 48	238 ± 46	179 ± 17	43	18
	2008–2009	Neutral	103 ± 14	86 ± 16	100 ± 18	260 ± 42	296 ± 13	271 ± 3	157 ± 39	210 ± 19	172 ± 18	69	16
	2009–2010	El Niño	105 ± 10	86 ± 8	97 ± 13	249 ± 31	334 ± 10	273 ± 3	145 ± 31	249 ± 12	176 ± 11	29	14
	2010–2011	La Niña	82 ± 10	69 ± 11	116 ± 8	274 ± 21	313 ± 1	274 ± 1	192 ± 22	245 ± 11	159 ± 8	62	20
	2011–2012	La Niña	92 ± 20	ND	93 ± 10	240 ± 33	ND	278 ± 1	149 ± 38	ND	185 ± 11	32	ND
	Mean		90 ± 14	86 ± 12	102 ± 6	252 ± 17	292 ± 3	272 ± 2	163 ± 20	207 ± 11	171 ± 7	56 ± 19	17 ± 4
ANF	2002–2003	El Niño	72 ± 19	110 ± 8	91 ± 1	242 ± 20	289 ± 10	268 ± 1	170 ± 28	180 ± 3	177 ± 1	58	10
	2003–2004	Neutral	82 ± 15	99 ± 11	85 ± 1	259 ± 22	277 ± 7	268 ± 1	178 ± 23	179 ± 4	184 ± 1	54	11
	2004–2005	Neutral	77 ± 19	91 ± 3	86 ± 1	252 ± 20	270 ± 2	269 ± 1	176 ± 12	179 ± 2	184 ± 1	53	15
	2005–2006	Neutral	72 ± 19	87 ± 2	87 ± 1	244 ± 18	274 ± 2	268 ± 1	173 ± 24	188 ± 1	182 ± 1	49	16
	2006–2007	Neutral	64 ± 16	91 ± 2	84 ± 1	242 ± 14	274 ± 5	266 ± 1	178 ± 21	183 ± 3	183 ± 1	62	11
	2007–2008	La Niña	65 ± 13	94 ± 7	85 ± 2	251 ± 15	279 ± 5	269 ± 2	186 ± 15	185 ± 2	184 ± 1	58	14
	2008–2009	Neutral	70 ± 16	98 ± 3	86 ± 2	253 ± 18	282 ± 4	270 ± 1	183 ± 8	184 ± 2	184 ± 1	54	17
	2009–2010	El Niño	79 ± 18	100 ± 8	87 ± 1	251 ± 19	282 ± 9	268 ± 1	173 ± 28	183 ± 3	181 ± 1	46	9
	2010–2011	La Niña	76 ± 18	103 ± 6	84 ± 1	255 ± 28	289 ± 4	267 ± 1	180 ± 20	187 ± 6	184 ± 1	47	11
	2011–2012	La Niña	77 ± 18	ND	87 ± 1	245 ± 23	ND	270 ± 1	168 ± 24	ND	184 ± 1	27	ND
	Mean		73 ± 9	97 ± 5	86 ± 1	249 ± 17	280 ± 5	268 ± 1	176 ± 15	183 ± 1	183 ± 1	51 ± 10	13 ± 4

[a]The indexes were calculated using WA-ANF and WA-ALF methods. The number of Julian days representing the indexes refer to the 1 July (phenological year). The amplitude of Chl-a (mg m^{-3}) and ZET (m^2 s^{-1}) represent the accumulated magnitude value between the onset and end; the interannual variation in PAR amplitude was minimal (data not shown). ND = No Data.

(Figure 5b) and WA-ALF (Figure 5d), the values varied little with latitude, except for ZET onset calculated with WA-ALF, which indicates slightly earlier onset (~15 days) in the southern area (Table 3). For all of the variables, the duration of the annual cycle presented relatively higher variability with WA-ALF than with WA-ANF.

3.4. Coupling of Chl-a Annual Cycle and Phenology to Those of Environmental Variables

The results obtained from coherence WA (Figure 6) indicated that, in the region of study, the mean annual Chl-a cycle (timing of the phytoplankton bloom) was mostly in phase with or coupled to those of ZET (timing of the spring-summer upwelling period) and PAR (timing of spring-summer increase in PAR intensity). In contrast, the mean annual cycle of SST (timing of the spring-summer increase in SST) lagged that of Chl-a; this lag amounted ~55–60 days, as derived from the phenological indexes in Table 3. The extent of the coupling of Chl-a with ZET and PAR from the WA-derived phenological indexes are shown in Tables 2 and 3. The mean time-space onsets of the Chl-a and PAR cycles were similar (<15 days differences); those for Chl-a and ZET were also similar with the WA-ALF, but not with WA-ANF calculation, with Chl-a starting ~24 days earlier than that of ZET. The mean end dates for Chl-a and PAR cycles were relatively similar (≤20 days later for PAR) but not between Chl-a and ZET cycles (31–42 days later for ZET), independently of the WA frequency bands used. The mean durations of the cycles were similar for these three variables when using WA-ANF and WA-ALF calculations, except that the ZET cycle lasted ~44 days longer than that of Chl-a with the latter approach.

3.5. Interannual Variability in the Phenology of Chl-a and Environmental Variables

During the time series analyzed in this study (2002–2012), one moderate (2002–2003) and one strong El Niño event (2009–2010) and three strong La Niña events (2007–2008, 2010–2011, and 2011–2012) were reported (http://www.cpc.noaa.gov/products/analysis_monitoring/ensostuff/ens). On this basis, the interannual changes in the mean phenology of Chl-a and the environmental variables SST, ZET, and PAR were analyzed for the indexes obtained with WA and other methods. In the search for differences, the uncertainty of ~15 days in index estimates for Chl-a (see section 2.2) was taken into account.

Compared to the mean time-space phenology of Chl-a, the indexes for onset, end, and duration calculated with WA-ANF indicated that interannual variation during the period of study was minimal, as it was for the

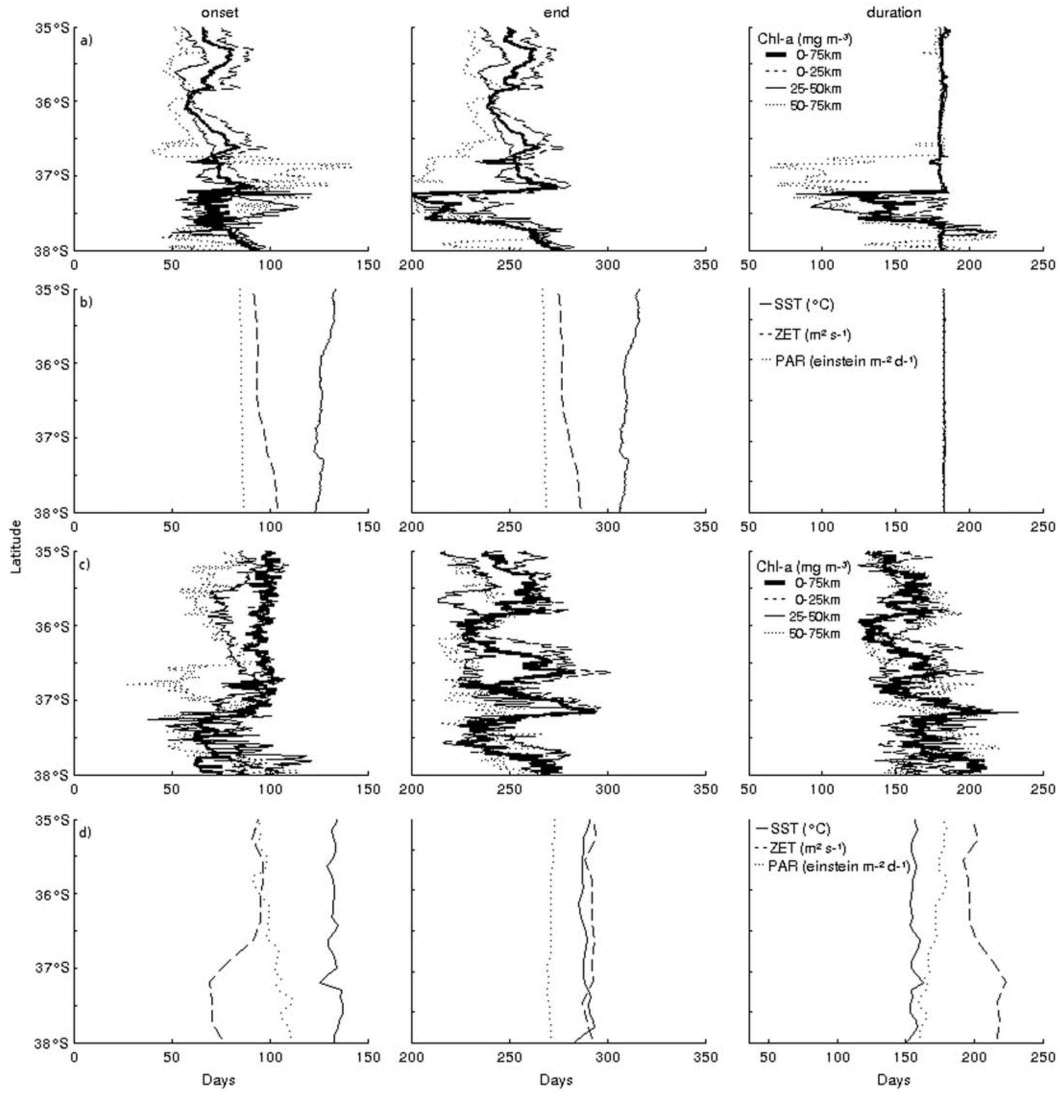

Figure 5. Latitudinal variability in the phenological indexes (onset, end, and duration) using (a and b) the ANF and (c and d) the ALF frequency bands. In the case of Chl-a (Figures 5a and 5c), the values include the mean zonal values (0–75 km, thick solid line) and those for three sections (0–25 km: dashed line; 25–50 km: thin solid line; 50–75 km: dotted line). The mean zonal values for SST (solid line), PAR (dotted line), and ZET (dashed line) are represented in Figures 5b and 5d.

ZET and PAR indexes (Table 2). With WA-ALF, the most significant difference from the mean value was for Chl-a duration during La Niña 2010–2011 (∼1 month longer); lesser differences were detected in 2005–2006 (∼17 days longer) and El Niño 2009–2010 (∼18 days shorter). In contrast to these WA results, Chl-a onset as estimated by the threshold method detected earlier onsets (∼1 month) in 2006–2007 and La Niña 2007–2008 (Table 1). In the case of PAR, interannual variability in the indexes was minimal with WA (Table 2) whereas for ZET, WA-ANF did not detect index variations but WA-ALF and the cumulative sum method did (Tables 1 and 2). The latter two coincided in some cases; the duration was shorter than the mean value in El Niño 2002–2003 and in 2003–2004, and it was longer in El Niño 2009–2010 and La Niña 2010–2011. These differences were greater (∼56–86 days) with the cumulative sum method than with WA-ALF (∼35–42 days).

In terms of interannual variability in Chl-a amplitude (accumulated magnitude during the productive period), the mean index values were similar with WA-ANF but more variable with WA-ALF (Table 2). In both cases, the values were lower during La Niña 2011–2012 but WA-ALF also detected a lower amplitude in El Niño 2009–2010 and higher values in El Niño 2002–2003 and in 2006–2007. In contrast, the amplitude values for ZET remained similar throughout the time series (Table 2).

Table 3. Comparison of the Onset and End Indexes for Chl-a, ZET, SST, and PAR Estimated for the Region of Study and in Two Areas Within the Region of Study[a]

Method	Area	Chl-a	ZET	SST	PAR
Onset					
ANF	35°S–38°S	73 ± 9	97 ± 5	128 ± 4	86 ± 1
		11 Sep	5 Oct	5 Nov	24 Sep
	35°S–37.2°S	73 ± 8	96 ± 3	130 ± 4	87 ± 1
		11 Sep	4 Oct	7 Nov	25 Sep
	37.2°S–38°S	77 ± 9	105 ± 1	127 ± 2	88 ± 1
		15 Sep	13 Oct	4 Nov	26 Sep
ALF	35°S–38°S	90 ± 14	86 ± 12	133 ± 4	102 ± 6
		28 Sep	24 Sep	10 Nov	10 Oct
	35°S–37.2°S	98 ± 5	89 ± 9	133 ± 4	101 ± 5
		3 Oct	27 Sep	10 Nov	9 Oct
	37.2°S–38°S	69 ± 5	74 ± 4	136 ± 3	111 ± 2
		7 Sep	12 Sep	13 Nov	19 Oct
End					
ANF	35°S–38°S	249 ± 17	280 ± 5	311 ± 4	268 ± 1
		6 Mar	6 Apr	7 May	25 Mar
	35°S–37.2°S	254 ± 8	279 ± 3	313 ± 4	269 ± 1
		11 Mar	5 Apr	9 May	26 Mar
	37.2°S–38°S	239 ± 26	287 ± 1	310 ± 2	270 ± 1
		24 Feb	13 Apr	6 May	27 Mar
ALF	35°S–38°S	252 ± 17	292 ± 3	289 ± 3	272 ± 2
		9 Mar	18 Apr	15 Apr	29 Mar
	35°S–37.2°S	255 ± 17	294 ± 2	290 ± 2	273 ± 2
		12 Mar	20 Apr	16 Apr	30 Mar
	37.2°S–38°S	249 ± 16	292 ± 3	291 ± 4	272 ± 1
		6 Mar	18 Apr	17 Apr	29 Mar

[a]The phenological indexes were identified using WA-ANF and WA-ALF methods for all the variables. The number of Julian days representing the indexes refer to the 1 July (phenological year); the corresponding dates are also shown below each case.

The relatively high dispersion of the mean values of the WA-derived indexes (Table 2) relates to their spatial variability (Figure 5), which needs to be taken into account in analyzing interannual variability. Figure 7 presents the anomalies in the onset, duration, and amplitude indexes for all the variables (calculated with WA-ALF but WA-ANF presented similar patterns) on a latitude basis. For Chl-a (Figure 7a), the anomalies were latitudinally coherent in some years (e.g., 2009–2010) and less so in others (e.g., 2005–2006); the location of the discontinuities in the anomaly pattern was not always the same. The environmental variables also displayed similar patterns, with spatial coherence in some years but not in others; also, the location of the discontinuities was not always the same (Figures 7b–7d).

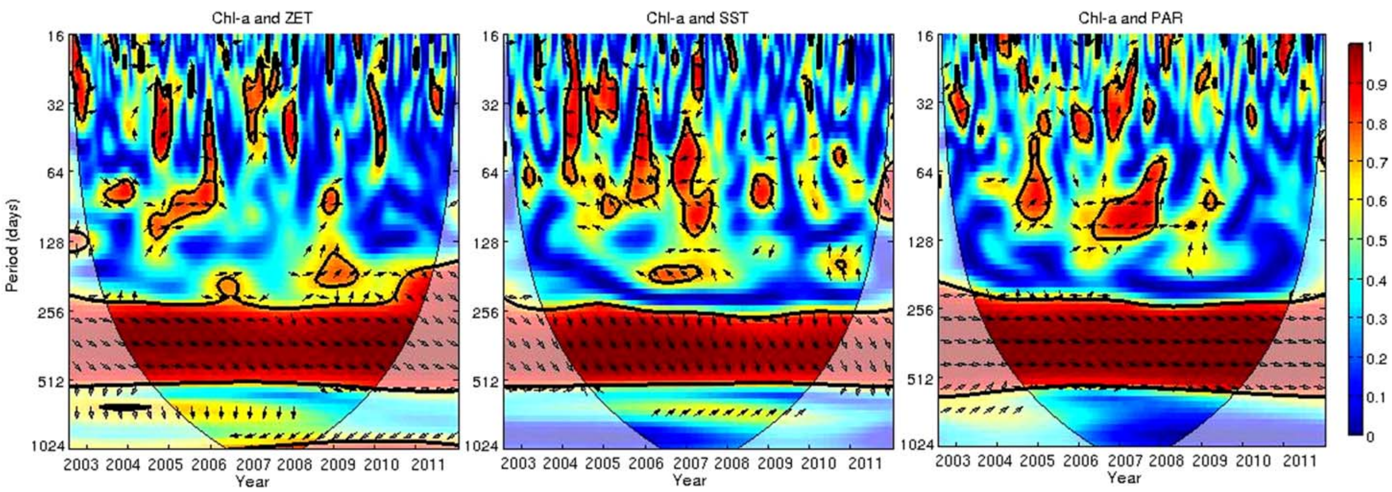

Figure 6. Cross-wavelet coherence spectra between (a) Chl-a and SST, (b) Chl-a and ZET, and (c) Chl-a and PAR in the region of study. Color indicates the level of covariability between the time series (values between 0 and 1); arrows denote the relative phase between the time series (right: in phase; left: antiphase; up or down: ones series leads the other by 90°). Black contours in the spectra indicate significant (Monte Carlo, 95% significance) covariability between two variables; the black curved line in the spectra depicts the cone of influence, outside of which edge effects become important.

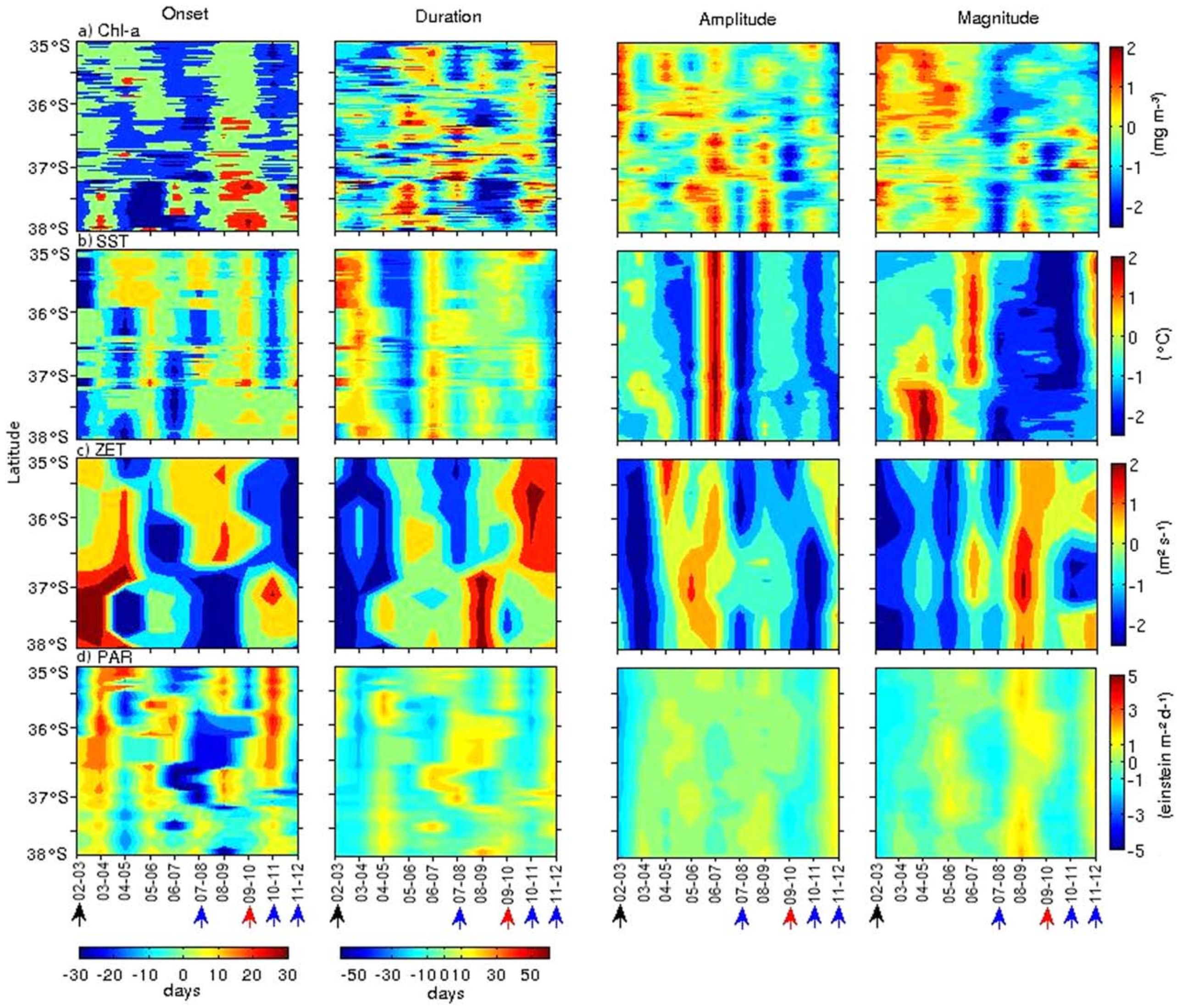

Figure 7. Latitudinal and interannual variability in the anomalies of phenological indexes in the region of study, including (first column) onset, (second column) duration, (third column) amplitude, and (fourth column) magnitude during the annual productive period (1 September year N to March year N + 1) for: (a) Chl-a, (b) ZET, (c) SST, and (d) PAR. The anomalies in onset and duration (days) are identified in the color bars located at the bottom of the figures; the anomalies in amplitude and magnitude are represented in the color bars on the right side (see sections 2.3 and 2.4 for definitions and details of calculation). The arrows at the bottom of the figures indicate the occurrence of ENSO conditions: moderate El Niño (black), strong El Niño (red), and strong La Niña (blue).

In terms of the mean anomalies in the magnitude of the variables during the productive period of each year (from September year N to March year N + 1, with one anomaly value per year; see section 2.4 for a description of its calculation), Chl-a values were spatially coherent (Figure 7a), with most of the positive values occurring during the first phase in the time series and negative values concentrated in La Niña 2007–2008. In the case of SST, mostly negative anomalies in magnitude were detected in the whole region during the second phase (i.e., after 2006) in the time series (Figure 7b). ZET anomalies were mostly positive (i.e., favorable for upwelling) during the same phase but with considerable spatial heterogeneity (Figure 7c). Interannual differences in magnitude for PAR were minimal (Figure 7d).

3.6. Interannual Differences in Chl-a Magnitude and Environmental Variables in Relation to Climate Variability

In order to obtain a general overview of the pattern of interannual variation in Chl-a magnitudes in the region of study, mean anomalies were estimated for each month in the productive period of each year

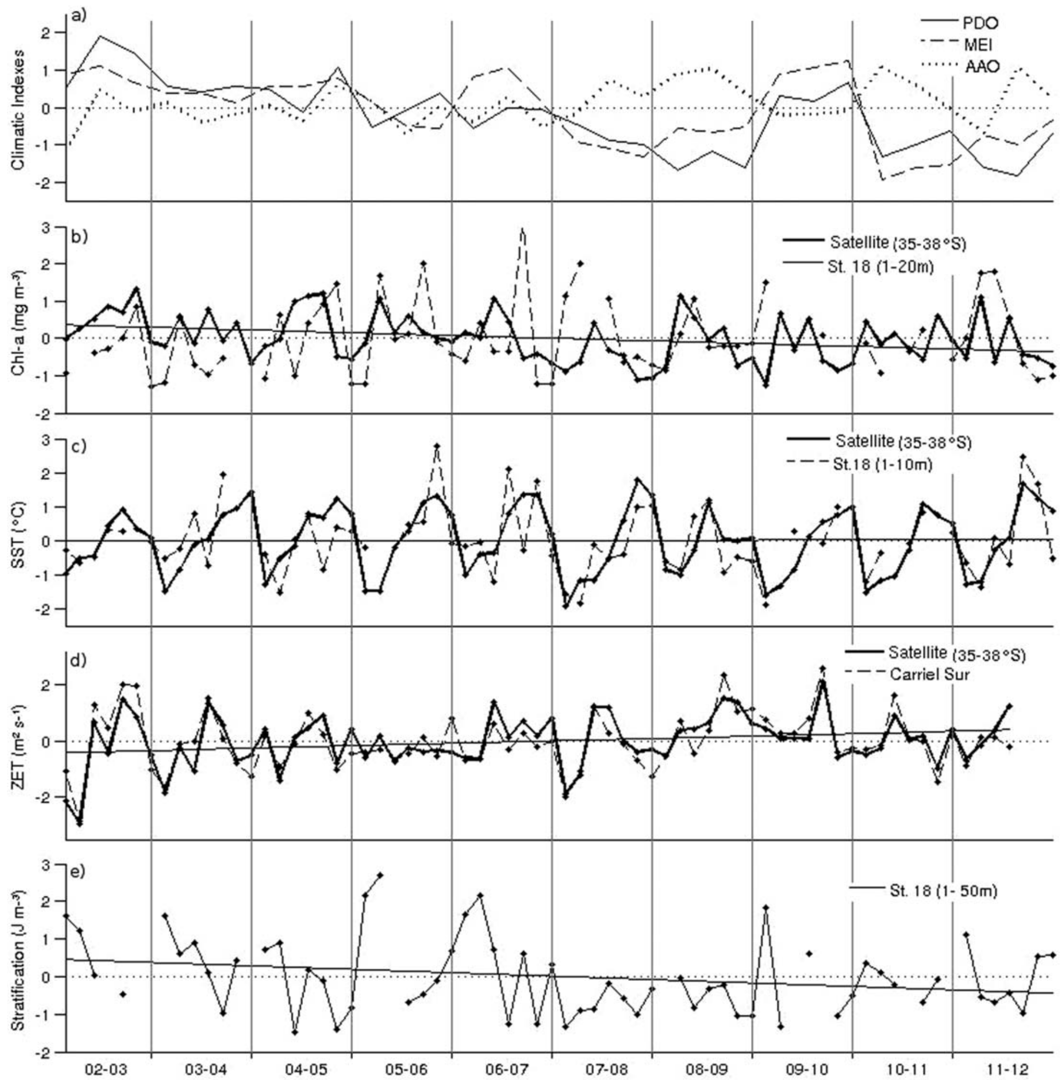

Figure 8. Distribution of (a) the climate indexes AAO, PDO, and MEI, and of the mean regional anomalies for each month during the productive period (1 September year N to March year N + 1; see section 2.4 for details of calculation) for: (b) Chl-a satellite and in situ monthly data from Station 18 (mean: 3.5 and 4.7 mg m^{-3}, respectively); (c) SST satellite and in situ monthly data from Station 18 (mean: 14.2 and 13.0°C, respectively); (d) ZET satellite and in situ monthly data based on winds obtained at Carriel Sur airport (mean: 0.57 and 0.12 m^{-2} s^{-1}, respectively); and (e) in situ monthly stratification index calculated from sigma-t data at Station 18 (mean: 50.6 J m^{-3}; positive anomalies indicate stronger stratification. The black lines across the time series denotes the linear trend in the data; significant trends were found for Chl-a, the stratification index ($p < 0.05$), and for ZET ($p < 0.10$) anomalies.

were estimated (seven monthly values per year; see section 2.4 for a description of the calculations). Satellite SST and ZET, and complementary in situ data from Station 18 were treated similarly (Figure 8). These results were analyzed in terms of the variations in the climate indexes MEI, PDO, and AAO (Figure 8a); the first two indexes were mostly positive to neutral from the beginning of the time series until 2006–2007 (first phase), after which they were mostly negative except for the El Niño 2009–2010 period (second phase). AAO was mostly neutral during the first phase and changed to mostly positive during the second, except for El Niño 2009–2010. No significant correlation (at lag = 0) was found between Chl-a magnitude anomalies in the region (0–75 km offshore band) and the climate indexes ($p > 0.10$).

The distributions of Chl-a and ZET magnitude anomalies displayed significant but opposite linear trends in the ~10 year time series, negative ($p < 0.01$) and positive ($p < 0.09$), respectively. A first phase (2002–2007) was characterized by positive Chl-a and negative ZET values (unfavorable or less favorable to upwelling), whereas a second phase (2008–2012) displayed mostly negative Chl-a and positive ZET values (Figures 8b and 8d). In contrast, SST magnitude anomalies were close to zero (Figure 8c). A calculation of the frequency and length of upwelling events during the productive period showed no differences between the two phases (data not shown).

The in situ ZET and SST data showed the same patterns as the satellite data but the in situ Chl-a data were less consistent with the satellite data. However, the SST and Chl-a in situ data consist of single monthly values, whereas the satellite data provide wider monthly coverage, even with the gaps in these time series. The in situ water column stratification index, using density data from Station 18, showed a trend of negative anomalies ($p < 0.05$), with mostly positive values in the first phase and negative values in the second (Figure 8e). In summary, lower Chl-a magnitude values during the second phase of the 2002–2012 time series coincided with lower water column stratification and higher ZET magnitudes (Figure 8). As well, the SST amplitude was lower during this period (Figure 7b). This second phase was represented by mostly negative MEI and PDO and positive AAO values, except for El Niño 2009–2010 (Figure 8a).

4. Discussion

This study evaluated the annual cycle and estimated the phenological indexes of phytoplankton (satellite-derived Chl-a), their time-space variations, and their coupling to the annual cycles and phenologies of environmental forcing in the coastal upwelling region between 35°S and 38°S. Previous studies in this region have described the generalities of the annual phytoplankton cycle and its link to local wind forcing in qualitative [e.g., *Strub et al*., 1998; *Atkinson et al*., 2002] and quantitative terms [*Morales et al*., 2013] but not in terms of phenological metrics. We first discuss the problems associated with the estimation of these metrics using different methods and/or frequency bands, and their effect on evaluating coupling between Chl-a and environmental forcing, and in the assessment of interannual variability in the indexes. Second, we discuss the spatial heterogeneity in the Chl-a phenological indexes, its effect on the evaluation of interannual shifts in response to climate variability, and the processes that might influence the trend observed in the magnitude of Chl-a and environmental variables in the ~10 year time series.

4.1. Phenological Indexes: Methods of Calculation and Implications on the Results

The method used in the identification of the phenological indexes in the annual cycle of Chl-a has been shown to affect results, at least in the case of onset estimation [*Brody et al*., 2013]. The most commonly used techniques for bloom onset identification are the threshold method (with or without accumulated sum of values) and the rate of change method, or a mixture of the two [*Ji et al*., 2010; *Racault et al*., 2012; *Brody et al*., 2013]. The rate of change method has been described as more objective because, unlike the threshold method, it does not require the selection of a unique value or percentage to estimate onset [*Rolinski et al*., 2007]. However, the use of different curve fitting models in the rate of change method can produce differences in the results [*Rolinski et al*., 2007; *Verbesselt et al*., 2010]. In the threshold method, differences can arise from biases in the identification of the onset of the annual bloom when using high-frequency and outlier data in the analysis, and from changing the start of the phenological year [*Brody et al*., 2013]. The timing of missing data also has a significant effect [*Cole et al*., 2012]. In contrast to these methods, WA allows for decomposing the time series with respect to time and frequencies of variability in a given signal and does not assume stationarity in the periodic process [*Percival and Walden*, 2000]. In this sense, it is more objective than other spectral methods that make this assumption [*Hudson*, 2010]. As with the rate of change method, WA indexes are derived from the change of phase in the curves reconstructed with the values of the time series [*Rolinski et al*., 2007; *White et al*., 2009; *Verbesselt et al*., 2010].

In this study, WA was applied to identify the phenological indexes for two different frequency bands, WA-ANF and WA-ALF. We used WA-ANF in the first place because we assumed that the annual frequency band alone would be sufficient for index identification. However, as a comparison with other methods, we also included all the frequencies except the synoptic (WA-ALF) in the calculations. Our results show that index estimation (onset, end, and duration) using WA is dependent upon the frequency bands included in the analyses (Tables 2 and 3). As well, the WA-ALF calculation of mean time-space index values provided similar results to those of other methods using a similar frequency band (Table 1 and Figure 4). Moreover, the pattern of change in the indexes with the two calculations was different among the variables; for example, Chl-a and PAR mean onset dates were earlier with WA-ANF than with WA-ALF, but it was the reverse for ZET onset. This implies that the assessment of the coupling between the annual cycle and phenology of Chl-a and those of potential environmental forcing can produce different results depending on the frequency bands used in the calculations, as was the case with ZET (Table 2).

A similar onset for Chl-a and ZET with WA-ALF supports the view that the initiation of the Chl-a bloom is determined by an accumulation of a series of higher-frequency wind events favorable to upwelling and/or intense enough to produce significant input of nutrients to the euphotic layer (a preconditioning). The similarity in the onset of Chl-a bloom and the upwelling season has also been ascertained for the California Current System when all frequencies except the synoptic (<8 days) were included in the estimation with the threshold method [*Henson and Thomas*, 2007a]. Recently, the period of winter/spring upwelling, in contrast to that of the spring/summer when upwelling is greatest, has been found to be more relevant to pelagic productivity in the California Current System, suggesting that oceanographic conditions leading up to the spring transition are more critical than the spring transition date [*García-Reyes et al*., 2013]. In this context, winter preconditioning of the Chl-a annual bloom cycle is a topic in the region of this study deserves further research.

The mean onset of the annual Chl-a bloom was also similar to that of PAR (Figure 4 and Table 2), suggesting that both PAR and ZET contribute to triggering Chl-a bloom. The strengthening of south-westerly winds during the spring-summer period produces increased upwelling associated with nutrient fertilization of the photic layer, this being coincidental with a higher solar radiation in the region of study [*Hernández et al*., 2012]. On the other hand, the onsets of the annual Chl-a bloom and the SST cycle were uncoupled regardless of the method of calculation (Figure 4 and Table 3). This uncoupling has been reported by *Morales et al*. [2013] for the region between 33°S and 42°S. *Racault et al*. [2012] recently proposed that Chl-a onset in coastal upwelling regions is highly associated with the onset of upwelling activity and weakly with those of PAR and SST, which is in contrast to our results (Figure 6).

Other potential forcing factors triggering the onset of the Chl-a annual bloom have been proposed for different regions, including: (i) water column stratification [*Tian et al*., 2011; *Zhai et al*., 2011]; (ii) mixed-layer depth [*Platt et al*., 2009; *Lavigne et al*., 2013]; and (iii) horizontal and vertical mixing [*Kim et al*., 2009; *Tian et al*., 2011]. On the other hand, the end date of the Chl-a bloom was mostly different from those for SST, ZET, and PAR, suggesting that they were not determinants of bloom termination (Figure 4 and Tables 2 and 3). Nutrient depletion and/or grazing have been suggested as forcing factors for ending the annual Chl-a cycle [*Henson and Thomas*, 2007b; *Wiltshire et al*., 2008; *Schlüter et al*., 2012], as well as reduced light and water-column destratification [*Racault et al*., 2012]. In general, much less attention has been given to the causes of the end of annual phytoplankton blooms, which, along with bloom duration, requires further investigation.

Another implication in using different methods to estimate Chl-a phenological indexes concerns the assessment of interannual variability. Our results indicate that only a few shifts in phenological indexes were detected during the 2002–2012 time series with WA-ALF, but none with WA-ANF, and these shifts were not all ENSO-related (Figure 7 and Table 3). However, the mean indexes during El Niño 2009–2010 and La Niña 2010–2011 suggest a similar pattern to that described previously for ZET phenology in the region [*Montecinos and Gomez*, 2010], with later onset and shorter duration during El Niño and earlier onset and longer duration during La Niña. Most of this variability was, however, within the range of the uncertainty in index estimation (~15 days). The pattern of index shift also varied when comparing the WA-ALF and threshold methods, although both displayed a similar tendency for the onset during 2009–2010 and 2010–2011. The threshold method detected an earlier onset of Chl-a (~1 month difference with the mean value) during La Niña 2007–2008 and in 2006–2007, while with the WA method these differences were <10 days (Tables 1 and 2).

4.2. Spatial and Temporal Changes in Chl-a Phenology and Bloom Magnitude

The region between 35°S and 38°S displays spatial variability in phytoplankton seasonality (Figure 3) and phenological indexes (Table 3 and Figure 5). The greatest variations occurred between the northern (35°S–37°S) and the southern areas (~37°S–38°S). They may be related to differences in coastline orientation and shelf width [*Morales et al*., 2013], which contribute to variations in wind patterns that in turn generate differences in coastal upwelling processes, as has been shown for other coastal upwelling systems [e.g., *Prego et al*., 2012]. Results of numerical models indicate that in the region of study coastal upwelling is more intense and the shelf narrower in the southern area than in the northern [*Mesias et al*., 2003], the conditions in the former being less favorable for Chl-a growth/accumulation. On the other hand, large enclosed areas like the Gulf of Arauco are characterized by slower water circulation, which could favor phytoplankton growth/accumulation, as has been shown for other coastal upwelling systems [*Barth et al*., 2005]. In both situations, the Chl-a annual cycle was weak (Figure 3). River discharge could also influence phytoplankton phenology by supplying additional nutrients [*Tweddle et al*., 2010; *Jutla et al*., 2011], but no effects associated with the Itata or Bio-Bio Rivers were detected in this study.

The use of high-resolution time series in this study demonstrated a spatially complex pattern in Chl-a phenology (Figures 5 and 7), which precludes a simple description of the effects of interannual variability in the indexes associated with climate events during the period of study. Similar spatial variations have recently been reported for other ocean regions. *Sasaoka et al*. [2011] found that the onset of the spring bloom in a specific area of the subarctic North Pacific was earlier in the El Niño phase and later in La Niña phase, whereas the pattern was reverse in an adjacent area. *Foukal and Thomas* [2014] also found geographic differences in relation to interannual variability in the seasonal cycle of Chl-a across the California Current system, with some areas being more stable than others, though a spatially coherent variation was associated with strong basin-scale events, including the 1997–1999 ENSO signal and the 2005 delayed spring transition. In connection with this spatial complexity, *Thomas et al*. [2009] described a strong latitudinal variation in the linkage between the anomalies in Chl-a magnitude and local/remote forcing in the California and the Humboldt upwelling systems. For the region of our study, they found a weak correlation ($r < 0.2$; $p > 0.05$) between monthly anomalies in Chl-a values and the upwelling index, whereas the association was strongly positive south of $\sim 38°$S and strongly negative north of $20°$S.

In accordance with canonical models, El Niño events (positive MEI) and warm PDO phases (positive PDO) have been associated with reduced Chl-a magnitude in upwelling systems, except in some regions. In the region of our study, Chl-a magnitude anomalies were negatively correlated (at lag = 0) with PDO (-0.2 to -0.4) and MEI (-0.4 to -0.6) during the 1997–2007 time series of satellite data [*Thomas et al*., 2009]. Our results do not support this pattern since mean satellite Chl-a anomalies were mostly positive during the first phase (2002–2007), when MEI and PDO were positive or neutral, and mostly negative during the second (2008–2012), when MEI and PDO were mostly negative except for El Niño 2009–2010 (Figures 8a and 8b). More specifically, Chl-a magnitude and amplitude anomalies were the lowest during La Niña 2007–2008 and El Niño 2009–2010 and were not directly related to changes in SST or ZET anomalies during the productive period (Figure 7). The annual cycle during La Niña 2007–2008 was unusual in that SST winter-spring values were the lowest of the time series and ZET favoring upwelling was sustained throughout the phenological year (Figure 2).

Certainly, our 10 year time series is too short for trend analyses and it did not include a strong El Niño event, such as the one in 1997 which had important effects on the biological productivity in the region of study [*Gomez et al*., 2012]. However, the patterns described above for ZET are in concordance with parallel observations in the region of study that suggest a trend of wind intensification (combination of QuikSCAT/SeaWinds (October 2002 to November 2009) and MetOP/ASCAT (December 2009 to September 2013) scatterometers), as well as a trend of decreasing water column temperatures (0–80 m; Station 18 data from 2002 to 2013) (W. Schneider, manuscript in preparation, 2014). *Aravena et al*. [2014] showed that the Bakun upwelling index has increased since 2010, after a decrease over the previous 10 years. Such intensification of winds has the potential to substantially increase coastal upwelling, a condition that appears to have been unfavorable for phytoplankton growth in the region of study. The mechanisms involved may include deeper mixing in the water column (dilution of biomass and/or reduced light) and/or increased offshore biomass transport. These results contrast with the expected pattern of increased phytoplankton biomass during La Niña events, which were the dominant condition during the second phase in our time series, in response to higher coastal upwelling intensity and shallower nutricline in the eastern South Pacific region [e.g., *Ochoa et al*., 2010] and other coastal upwelling systems [e.g., *Chavez et al*., 2003]. On the other hand, under a scenario of climate-change-related wind intensification in coastal upwelling regions, which has been observed in the California Current system during the 1998–2008 period [e.g., *García-Reyes and Largier*, 2010], the response of phytoplankton is likely to be complex and different among taxonomic and/or functional components [*Harley et al*., 2006].

Our results show that MEI and AAO were, for the most part, in opposite phases during the second part of the time series (Figure 8a). Can this pattern explain the variations in Chl-a magnitude during the 2002–2012 time series? There have been few studies of the effects of AAO on variations in phytoplankton biomass/productivity in subtropical zones of the southern hemisphere. *Lovenduski and Gruber* [2005] found that positive AAO (or SAM: Southern Annular Mode) is associated with easterly wind and warm SST anomalies in the subtropical zone and this, in turn, negatively correlates with Chl-a magnitude in the same zone, probably as a consequence of reduced light due to a deeper mixed layer. *Racault et al*. [2012] found that positive AAO is associated with a shorter phytoplankton growing period (duration index) in the 35°S–50°S zone, coinciding with reduced upwelling and supply of nutrients. To our knowledge, no information is available on the combined effects of climate indexes, like AAO and MEI, on phytoplankton. Nevertheless, *Rahn* [2012] showed that there is constructive and destructive interference between these indexes, such that their combination either enhance or cancel alongshore wind anomalies in the region off central Chile; specifically, a positive AAO and negative MEI (La Niña) condition results in stronger positive alongshore wind anomalies. The latter appears to have been the dominant condition during the second phase in our time series and may explain the trend toward lower Chl-a bloom magnitudes, which combines with lower stratification and more intense upwelling (Figure 8). We argue that in the context of climate-change-related increase in ZET in this coastal upwelling region, fluctuations in Chl-a phenology and in the magnitude of the annual bloom will depend on the combined effects of climate indexes. On the other hand, local effects may have a stronger influence on these fluctuations compared to remote forcing.

5. Conclusions

A fine-scale resolution analysis of the annual cycle and phenology of satellite Chl-a and environmental variables (SST, ZET, and PAR) in the coastal upwelling region off central-southern Chile (35°S–38°S) for the period between mid-2002 and mid-2012 revealed that:

1. There is submeso and mesoscale variability in Chl-a annual cycle and phenology, which appears to be indirectly influenced by changes in coastline orientation and shelf width. However, the mean time-space values for the region of study indicate that the annual cycle in the first 50 km from the coast is marked and this pattern influences the mean phenological indexes.
2. WA analysis applied to accumulated data in this study can be a most appropriate method to derive phenological indexes in the case of Chl-a. In comparison with other common methods (e.g., threshold and rate of change), it allows to objectively derive not only the onset but other indexes, and it does not assume stationarity in the time series as most spectral methods do.
3. The mean annual cycle of Chl-a is, for the most part, coupled or coherent with those of PAR and ZET. When all frequencies longer than the synoptic were used in the analysis (WA-ALF), the onset dates of Chl-a, ZET, and PAR were similar whereas with the annual band approach (WA-ANF), ZET lagged Chl-a by ~20 days. The annual SST cycle lagged that of Chl-a by ~2 months, independent of the WA frequencies used in the calculations.
4. Interannual variability in mean Chl-a phenology (e.g., onset, duration, and amplitude) calculated with WA was relatively undetectable during the period of study, except that a longer duration of the productive period (~1+ month compared with the mean value) was observed during La Niña 2010–2011 year (WA-ALF).
5. Chl-a magnitude anomalies during the productive period of the ~10 year time series displayed a negative trend, while the trend was positive for ZET. The Chl-a trend differs from the pattern expected under ENSO-influence, since three La Niña events took place during the second phase (2008–2012).

Acknowledgments
Data analyses and preparation of the manuscript were supported by the FONDECYT Project 1120504 (CONICYT-Chile) to C.E.M. and S.H. Additional support during the writing phase was provided by the Instituto Milenio de Oceanografía (IMO-Chile), funded by the Iniciativa Científica Milenio (ICM-Chile). The authors thank the Ocean Biology Processing Group (Code 614.2) at the Goddard Space Flight Center, Greenbelt, MD 20771, for the production and distribution of the ocean color data. Chl-a, SST, and PAR data are produced by Remote Sensing Systems and sponsored by the NASA Earth Science MODIS Project (http://oceancolor.gsfc.nasa.gov/). Surface wind data were obtained by Remote Sensing Systems and sponsored by the NASA Earth Science MEaSUREs DISCOVER Project (CCMP; http://podaac.jpl.nasa.gov/). We are grateful to the COPAS center for providing in situ oceanographic data (temperature and salinity) from Station 18 time series. The comments provided by two anonymous reviewers greatly improved the interpretation of our results and generated relevant changes in the original MS. A.C.A. was supported by a Universidad de Concepción graduate scholarship (2011–2013), funds from FONDECYT 1120504, and a CONICYT-Chile Scholarship (2013). S.H. was partially funded by FONDECYT 1131047 and M.C.R. by FONDECYT 11130463. This publication is a contribution to the REDOC (MECESUP) Project at the University of Concepción and to the IMO-Chile.

References

Alvera-Azcárate, A., A. Barth, M. Rixen, and J. M. Beckers (2005), Reconstruction of incomplete oceanographic data sets using empirical orthogonal functions: Application to the Adriatic Sea, *Ocean Modell.*, *9*, 325–346, doi:10.1016/j.ocemod.2004.08.001.
Alvera-Azcárate, A., A. Barth, J. M. Beckers, and R. H. Weisberg (2007), Multivariate reconstruction of missing data in sea surface temperature, chlorophyll, and wind satellite fields, *J. Geophys. Res.*, *112*, C03008, doi:10.1029/2007JC004243.
Alvera-Azcárate, A., A. Barth, D. Sirjacobs, F. Lenarts, and J.-M. Beckers (2011), Data interpolating empirical orthogonal functions (DINEOF): A tool for geophysical data analyses, *Mediter. Mar. Sci.*, *12*(3), 5–11.
Aravena, G., B. Broitman, and N. C. Stenseth (2014), Twelve years of change in coastal upwelling along the central-northern coast of Chile: Spatially heterogeneous responses to climatic variability, *PLoS ONE 9*(2), e90276, doi:10.1371/journal.pone.0090276.

Atkinson, L. P., A. Valle-Levinson, D. Figueroa, R. de Pol-Holz, V. A. Gallardo, W. Schneider, J. L. Blanco, and M. Schmidt (2002), Oceanographic observations in Chilean coastal waters between Valdivia and Concepcion, *J. Geophys. Res.*, *107*(C7), doi:10.1029/2001JC000991.

Bakun, A., and C. S. Nelson (1991), The seasonal cycle of wind stress curl in sub-tropical boundary current regions, *J. Phys. Oceanogr.*, *21*, 1815–1834, doi:10.1175/1520-0485(1991).

Barth, J. A., S. D. Pierce, and T. J. Cowles (2005), Mesoscale structure and its seasonal evolution in the northern California Current System, *Deep Sea Res., Part II*, *52*(1–2), 5–28, doi:10.1016/j.dsr2.2004.09.026.

Beckers, J. M., and M. Rixen (2003), EOF calculations and data filling from incomplete oceanographic data sets, *J. Atmos. Oceanic Technol.*, *20*(12), 1839–1856, doi:10.1175/1520-0426(2003).

Bograd, S. J., I. Schroeder, N. Sarkar, X. Qiu, W. J. Sydeman, and F. B. Schwing (2009), Phenology of coastal upwelling in the California Current, *Geophys. Res. Lett.*, *36*, L01602, doi:10.1029/2008GL035933.

Brody, S. R., M. S. Lozier, and J. P. Dunne (2013), A comparison of methods to determine phytoplankton bloom initiation, *J. Geophys. Res. Oceans*, *118*, 2345–2357, doi:10.1002/jgrc.20167.

Carl, G., D. Doktor, D. Koslowsky, and I. Kuhn (2013), Phase difference analysis of temperature and vegetation phenology for beech forest: A wavelet approach, *Stochastic Environ. Res. Risk Assess.*, *27*, 1221–1230, doi:10.1007/s00477-012-0658-x.

Cazelles, B., M. Chavez, D. Berteaux, F. Ménard, J. O. Vick, S. Jenouvrier, and N. C. Stenseth (2008), Wavelet analysis of ecological time series, *Oecologia*, *156*, 287–304, doi:10.1007/s00442-008-0993-2.

Chavez, F. P., J. Ryan, S. E. Lluch-Cota, and C. M. Ñiquen (2003), From anchovies to sardines and back: Multidecadal change in the Pacific Ocean, *Science*, *299*, 217–221, doi:10.1126/science.1075880.

Cole, H., S. Henson, A. Martin, and A. Yool (2012), Mind the gap: The impact of missing data on the calculation of phytoplankton phenology metrics, *J. Geophys. Res.*, *117*, C08030, doi:10.1029/2012JC008249.

Correa-Ramirez, M. A., S. Hormazabal, and C. E. Morales (2012), Spatial patterns of annual and interannual surface chlorophyll-a variability in the Peru–Chile Current System, *Prog. Oceanogr.*, *92*(1), 8–17, doi:10.1016/j.pocean.2011.07.008.

Edwards, M., and A. J. Richardson (2004), Impact of climate change on marine pelagic phenology and trophic mismatch, *Nature*, *430*, 881–884, doi:10.1038/nature02808.

Escribano, R., and C. E. Morales (2012), Spatial and temporal scales of variability in the coastal upwelling and coastal transition zones off central-southern Chile (35–40°S), *Prog. Oceanogr.*, *92–95*, 1–7, doi:10.1016/j.pocean.2011.07.019.

Foukal, N. P., and A. C. Thomas (2014), Biogeography and phenology of satellite-measured phytoplankton seasonality in the California current, *Deep Sea Res., Part I*, *92*, 11–25, doi:10.1016/j.dsr.2014.06.008.

García-Reyes, M., and J. Largier (2010), Observations of increased wind-driven coastal upwelling off central California, *J. Geophys. Res.*, *115*, C04011, doi:10.1029/2009JC005576.

García-Reyes, M., W. J. Sydeman, B. A. Black, R. R. Rykaczewski, D. S. Schoeman, S. A. Thompson, and S. J. Bograd (2013), Relative influence of oceanic and terrestrial pressure systems in driving upwelling-favorable winds, *Geophys. Res. Lett.*, *40*, 5311–5315, doi:10.1002/2013GL057729.

Gomez, F., A. Montecinos, S. Hormazabal, L. A. Cubillos, M. A. Correa-Ramirez, and F. P. Chavez (2012), Impact of spring upwelling variability off southern-central Chile on common sardine (*Strangomera bentincki*) recruitment, *Fish. Oceanogr.*, *21*, 405–414, doi:10.1111/j.1365–2419.2012.00632.x.

Grinsted, A., J. C. Moore, and S. Jevrejeva (2004), Application of the cross wavelet transform and wavelet coherence to geophysical time series, *Nonlinear Processes Geophys.*, *11*, 561–566, doi:10.5194/npg-11–561-2004.

Harley, C. D. G., A. R. Hughes, K. M. Hultgren, B. G. Miner, C. J. B. Sorte, C. S. Thornber, L. F. Rodriguez, L. Tomanek, and S. L. Williams (2006), The impacts of climate change in coastal marine systems, *Ecol. Lett.*, *9*, 228–241, doi:10.5194/npg-11–561-2004.

Henson, S. A., and A. C. Thomas (2007a), Interannual variability in timing of bloom initiation in the California Current System, *J. Geophys. Res.*, *112*, C08007, doi:10.1029/2006JC003960.

Henson, S. A., and A. C. Thomas (2007b), Phytoplankton scales of variability in the California Current System: 1. Interannual and cross-shelf variability, *J. Geophys. Res.*, *112*, C07017, doi:10.1029/2006JC004039.

Hernández, K., B. Yannicelli, A. Montecinos, M. Ramos, H. González, and G. Daneri (2012), Temporal variability of incidental solar radiation and modulating factors in a coastal upwelling area (36°S), *Prog. Oceanogr.*, *92–95*, 18–32, doi:10.1016/j.pocean.2011.07.011.

Hudson, I. (2010), Interdisciplinary approaches: Towards new statistical methods for phenological studies, *Clim. Change*, *100*, 143–171, doi:10.1007/s10584-010-9859-9.

Ji, R., M. Edwards, D. Mackas, J. Runge, and A. Thomas (2010), Marine plankton phenology and life history in a changing climate: Current research and future directions, *J. Plankton Res.*, *32*(10), 1355–1368, doi:10.1093/plankt/fbq062.

Jutla, A. S., A. S. Akanda, J. K. Griffiths, R. Colwell, and S. Islam (2011), Warming oceans, phytoplankton, and river discharge: Implications for cholera outbreaks, *Am. J. Trop. Medicine Hyg.*, *85*, 303–308, doi:10.4269/ajtmh.2011.11–0181.

Kim, H., A. Miller, J. McGowan, and M. Carter (2009), Coastal phytoplankton blooms in the Southern California Bight, *Prog. Oceanogr.*, *82*, 137–147, doi:10.1016/j.pocean.2009.05.002.

Land, P. E., J. D. Shutler, T. Platt, and M. F. Racault (2014), A novel method to retrieve oceanic phytoplankton phenology from satellite data in the presence of data gaps, *Ecol. Indicators*, *37*, 67–80, doi:10.1016/j.ecolind.2013.10.008.

Lavigne, H., F. D'Ortenzio, C. Migon, H. Claustre, P. Testor, M. Ribera d'Alcalá, R. Lavezza, L. Houpert, and L. Prieur (2013), Enhancing the comprehension of mixed layer depth control on the Mediterranean phytoplankton phenology, *J. Geophys. Res. Oceans*, *118*, 3416–3430, doi:10.1002/jgrc.20251.

Lovenduski, N. S., and N. Gruber (2005), Impact of the Southern Annular Mode on Southern Ocean circulation and biology, *Geophys. Res. Lett.*, *32*, L11603, doi:10.1029/2005GL022727.

Mesias, J. M., R. P. Matano, and P. Strub (2003), Dynamical analysis of the upwelling circulation off central Chile, *J. Geophys. Res.*, *108*(C3), 3085, doi:10.1029/2001JC001135.

Miles, T., and R. He (2010), Temporal and spatial variability of Chl-a and SST on the South Atlantic Bight revisiting with cloud-free reconstructions of MODIS satellite images, *Cont. Shelf Res.*, *30*(18), 1951–1962, doi:10.1016/j.csr.2010.08.016.

Montecinos, A., and F. Gomez (2010), ENSO modulation of the upwelling season off southern-central Chile, *Geophys. Res. Lett.*, *37*, L02708, doi:10.1029/2009GL041739.

Morales, C. E., S. Hormazabal, I. Andrade, and M. A. Correa-Ramirez (2013), Time-space variability of chlorophyll-a and associated physical variables within the region off Central-Southern Chile, *Remote Sens.*, *5*(11), 5550–5571, doi:10.3390/rs5115550.

Ochoa, N., M. H. Taylor, S. Purca, and E. Ramos (2010), Intra- and interannual variability of nearshore phytoplankton biovolume and community changes in the northern Humboldt Current system, *J. Plankton Res.*, *32*(6), 843–855, doi:10.1093/plankt/fbq022.

Percival, D., and A. Walden (2000), *Wavelet Methods for Time Series Analysis*, Cambridge Univ. Press, N. Y.

Platt, T., and S. Sathyendranath (2008), Ecological indicators for the pelagic zone of the ocean from remote sensing, *Remote Sens. Environ.*, *112*, 3426–3436, doi:10.1016/j.rse.2007.10.016.

Platt, T., G. N. White III, L. Zhai, S. Sathyendranath, and R. Shovonlal (2009), The phenology of phytoplankton blooms: Ecosystem indicators from remote sensing, *Ecol. Modell.*, *220*, 3057–3069, doi:10.1016/j.ecolmodel.2008.11.022.

Prego, R., M. Varela, M. deCastro, N. Ospina-Alvarez, C. Garcia-Soto, and M. Gómez-Gesteira (2012), The influence of summer upwelling at the western boundary of the Cantabrian coast, *Estuarine Coastal Shelf Sci.*, *98*, 138–144, doi:10.1016/j.ecss.2011.12.009.

Racault, M., C. Le Quéré, E. Buitenhuis, S. Sathyendranath, and T. Platt (2012), Phytoplankton phenology in the global ocean, *Ecol. Indicators*, *14*, 152–163, doi:10.1016/j.ecolind.2011.07.010.

Racault, M., T. Platt, S. Sathyendranath, E. Ağirbaş, V. Martinez, and R. Brewin (2014), Plankton indicators and ocean observing systems: Support to the marine ecosystem state assessment, *J. Plankton Res.*, *36*(3), 621–629, doi:10.1093/plankt/fbu016.

Rahn, D. A. (2012), Influence of large scale oscillations on upwelling-favorable coastal wind off central Chile, *J. Geophys. Res.*, *117*, D19114, doi:10.1029/2012JD018016.

Rolinski, S., H. Horn, T. Petzoldt, and L. Paul (2007), Identifying cardinal dates in phytoplankton time series dates to enable the analysis of long-term trends, *Oecologia*, *153*, 997–1008, doi:10.1007/s00442-007-0783.

Sapiano, M., C. Brown, U. Schollaert, and M. Vargas (2012), Establishing a global climatology of marine phytoplankton phenological characteristics, *J. Geophys. Res.*, *117*, C08026, doi:10.1029/2012JC007958.

Sasaoka, K., S. Chiba, and T. Saino (2011), Climatic forcing and phytoplankton phenology over the subpolar North Pacific from 1998 to 2006, as observed from ocean color data, *Geophys. Res. Lett.*, *38*, L15609, doi:10.1029/2011GL048299.

Schlüter, M., A. Kraberg, and K. Wiltshire (2012), Long-term changes in the seasonality of selected diatoms related to grazers and environmental conditions, *J. Sea Res.*, *67*, 91–97, doi:10.1016/j.seares.2011.11.001.

Simpson, J. H., P. B. Tett, M. Argote-Espinosa, A. Edwards, K. J. Jones, and G. Savidge (1982), Mixing and phytoplankton growth around an island in a stratified sea, *Cont. Shelf Res.*, *1*, 15–31.

Strub, P., J. Mesías, V. Montecino, and J. Ruttlant (1998), Coastal ocean circulation off Western South America, in *The Sea*, vol. 11, edited by A. Robinson and K. Brink, pp. 273–313, John Wiley, N. Y.

Stuart, V., O. Ulloa, G. Alarcon, S. Sathyendranath, H. Major, E. J. Head, and T. Platt (2004), Bio-optical characteristics of phytoplankton populations in the upwelling system off the coast of Chile, *Rev. Chilena Hist. Nat.*, *77*, 87–105.

Thackeray, S. J., P. A. Henrys, I. D. Jones, and H. Feuchtmayr (2012), Eight decades of phenological change for a freshwater cladoceran: What are the consequences of our definition of seasonal timing?, *Freshwater Biol.*, *57*, 345–359, doi:10.1111/j.1365–2427.2011.02614.x.

Thomas, A. C., P. Brickley, and R. Weatherbee (2009), Interannual variability in chlorophyll concentrations in the Humboldt and California Current Systems, *Prog. Oceanogr.*, *83*, 386–392, doi:10.1016/j.pocean.2009.07.020.

Tian, T., J. Su, G. Floser, K. Wiltshire, and K. Wirtz (2011), Factors controlling the onset of spring blooms in the German Bight 2002–2005: Light, wind and stratification, *Cont. Shelf Res.*, *31*, 1140–1148, doi:10.1016/j.csr.2011.04.008.

Torrence, C., and G. P. Compo (1998), A practical guide to wavelet analysis, *Bull. Am. Meteorol. Soc.*, *79*, 61–78, doi:10.1175/1520-0477(1998).

Tweddle, J. F., et al. (2010), Relationships among upwelling, phytoplankton blooms, and phycotoxins in coastal Oregon shellfish, *Mar. Ecol. Prog. Ser.*, *405*, 131–145, doi:10.3354/meps08497.

Verbesselt, J., R. Hyndman, A. Zeileis, and D. Culvenor (2010), Phenological change detection while accounting for abrupt and gradual trends in satellite image time series, *Remote Sens. Environ.*, *114*, 2970–2980, doi:10.1016/j.rse.2010.08.003.

Wang, Y. Q., and D. Y. Liu (2014), Reconstruction of satellite chlorophyll-a data using a modified DINEOF method: A case study in the Bohai and Yellow seas, China, *Int. J. Remote Sens.*, *35*, 204–217, doi:10.1080/01431161.2013.866290.

White, M., et al. (2009), Intercomparison, interpretation, and assessment of spring phenology in North America estimated from remote sensing for 1982–2006, *Global Change Biol.*, *15*, 2335–2359, doi:10.1111/j.1365–2486.2009.01910.x.

Wiltshire, K. H., A. M. Malzahn, K. Wirtz, W. Greve, S. Janisch, P. Mangelsdorf, B. F. J. Manly, and M. Boersma (2008), Resilience of North Sea phytoplankton spring bloom dynamics: An analysis of long-term data at Helgoland Roads, *Limnol. Oceanogr.*, *53*(4), 1294–1302.

Winder, M., and J. Cloern (2010), The annual cycles of phytoplankton biomass, *Philos. Trans. R. Soc. B*, *365*, 3215–3226, doi:10.1098/rstb.2010.0125.

Yuras, G., O. Ulloa, and S. Hormazabal (2005), On the annual cycle of coastal and open ocean satellite chlorophyll off Chile (18–40°S), *Geophys. Res. Lett.*, *32*, L23604, doi:10.1029/2005GL023946.

Zhai, L., T. Platt, C. Tang, S. Sathyendranath, and R. H. Walls (2011), Phytoplankton phenology on the Scotian Shelf, *ICES J. Mar. Sci.*, *68*(4), 781–791, doi:10.1093/icesjms/fsq175.